Numerical Experiments with Multi-Models for Paleo-Environmental Problems

Project Representative
Ayako Abe-Ouchi Atmosphere and Ocean Research Institute, The University of Tokyo

Authors
Ayako Abe-Ouchi[*1], Masakazu Yoshimori[*2], Wing-Le Chan[*1], Akitomo Yamamoto[*1], Kazumi Ozaki[*1], Ryouta O'ishi[*3], Nitta Tomoko[*1], Takashi Obase[*1], Sam Sherriff Tadano[*1], Alexandre Laine[*3], Rumi Ohgaito[*4], Kunio Takahashi[*5] and Yujin Hamano[*2]

*1 Atmosphere and Ocean Research Institute, The University of Tokyo
*2 Faculty of Environmental Earth Science, Hokkaido University
*3 National Institute of Polar Research, Research Organization of Information and Systems
*4 Project Team for Risk Information on Climate Change, Japan Agency for Marine-Earth Science and Technology
*5 Department of Integrated Climate Change Projection Research, Japan Agency for Marine-Earth Science and Technology

The MIROC4m AOGCM was used for water hosing experiment to reproduce millennial scale climate change between stadial and interstadial. Results show climate change consistent with that of reconstruction from paleo proxy data. We developed a new method of downscaling to apply this climate change from AOGCM on a high-resolution AGCM. Coupled vegetation-AGCM experiments also show consistent vegetation change which is reconstructed from geological evidence. The effect of glacial ice sheet upon the Atlantic meridional overturning circulation (AMOC) is investigated by using AOGCM, AGCM and OGCM. The results show that the change in sea surface wind due to the glacial ice sheet contributes to the strengthening of the AMOC. Oceanic oxygen concentration change in the warm climate is estimated by running 2 and 4 times CO_2 experiments with AOGCM. The result shows decrease of O_2 in the first 500 years and finally a recovery to levels above that of the preindustrial. The strengthened AABW in the warm climate enhances ventilation and supplies oxygen-rich surface waters to the deep ocean. By using AOGCM results as boundary conditions, high resolution OGCM experiments are run focusing on Antarctica to estimate basal melting of Antarctic ice sheet in the LGM, preindustrial and doubled CO_2 environment. The results shows that the difference between basal melting in the doubled CO_2 environment and the pre-industrial is larger than the difference between those of the pre-industrial and LGM.

Keywords: atmosphere-ocean GCM MIROC, paleoclimate modeling, LGM, stadial/interstadial, oceanic oxygen, basal melting

1. Modeling stadial and interstadial climates of the last glacial period

1.1 Climate change between stadial and interstadial

Records from Greenland ice cores show that the last glacial period was characterized by climate fluctuations of millennial timescale [1], alternating between warm interstadials and cool stadials. These so-called Dansgaard-Oeschger events consist of a relatively rapid warming stage during which temperatures increase by about 8°C within a few decades, followed by a progressive cooling over a thousand years or so. It is believed that large amounts of meltwater from the Laurentide ice sheet led to discharge of freshwater into the North Atlantic Ocean and a weakening of the Atlantic meridional overturning circulation (AMOC), causing a decrease in northern hemisphere temperatures. Associated changes in climate may have been an important contributing factor, not only in species extinction eg Neanderthals, but also in the migration routes of modern humans [2].

To investigate how stadial climates differ to those of interstadial and its effect on the natural environment, we used MIROC3.2.3, an atmosphere-ocean general circulation model (AOGCM), to run a series of climate model experiments which included an artificial freshwater flux, or 'hosing', in the northern North Atlantic to eventually produce a cool stadial-like scenario. After a 500-year integration, the hosing was switched off and the experiment continued. For additional experiments, the sea-surface temperatures and sea ice were averaged over periods representing stadial and interstadial-like conditions (Fig. 1) and were then used to drive a medium and high resolution atmosphere general circulation model (AGCM), with orbital parameters and greenhouse concentrations set to a suitable configuration for time slices of interest.

The application of freshwater flux weakens the AMOC and produces an anti-symmetric change in temperature and precipitation in the two hemispheres (Fig. 2), with a southward shift of the intertropical convergence zone. This pattern is consistent with the bipolar seesaw phenomenon. Proxy data suggest a weakening of the Asian summer monsoons during stadial states. Both AOGCM and AGCM confirm this for the South Asian monsoon but wetter conditions prevail over parts of East Asia (Fig. 3). However, drier conditions in the AGCM appear to extend over much of the western Pacific, approaching the continent, especially with higher resolution. Longer model integration time for the high resolution AGCM may reduce annual variability and thus also model-data discrepancy.

Precipitation and surface air temperature from these various climate experiments were applied to the Lund-Potsdam-Jena dynamic global vegetation model (DGVM) to simulate changes in plant functional types (PFTs) which can be grouped as forest and grassland. In general, forest and grassland fraction changes are similar, irrespective of the climate model from which we obtain the precipitation and temperature data. Focusing on Europe, in the stadial state, forests reduce in the British Isles and throughout much of the continent where the forest loss is balanced by an increase in grassland (Fig. 4, top row). The reduction in temperate forests of western Europe and the reduction in boreal forests of northern Europe explain this total reduction in forest, despite an increase in boreal forests in western and central Europe as the lower temperatures favor these types. Total forest growth is limited to southern and eastern Spain and western Italy. By running the DGVM using just either the surface air temperature (Fig. 4, middle row) or precipitation (Fig. 4, bottom row) of the stadial climate, we were able to investigate their individual contributions to these changes in forest and grassland fraction. The distribution of these changes when only stadial temperature is applied resembles that of the stadial state (Fig. 4, top row), implying that temperature change is more important, and this is true for the individual

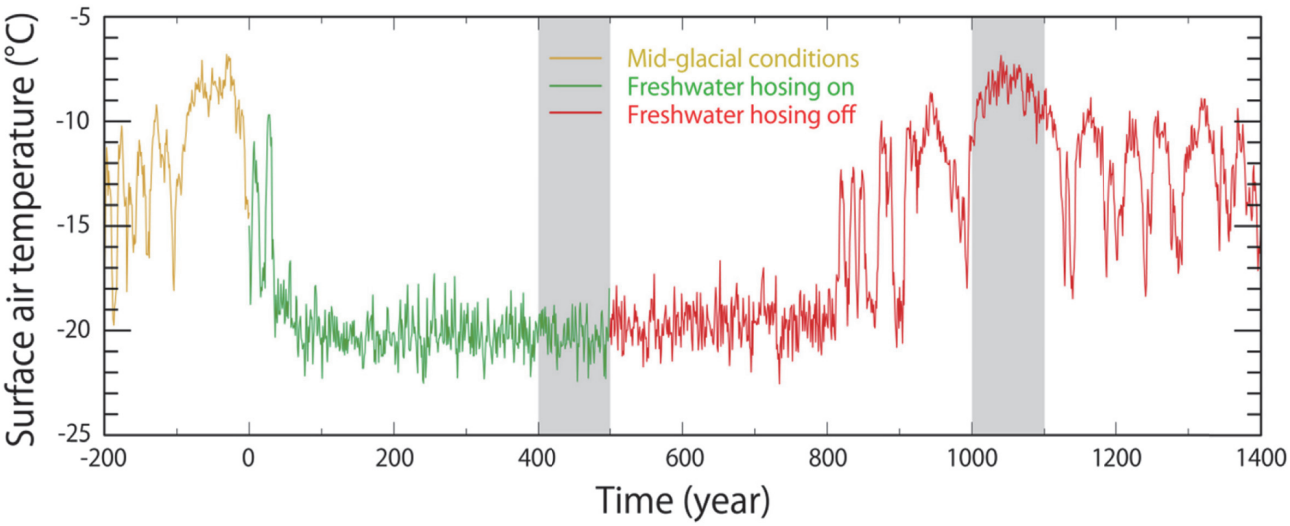

Fig. 1 Time series of the annual mean surface air temperature, averaged over the northern North Atlantic (70°W-10°E, 50°N-70°N) in experiments using the AOGCM. Freshwater flux is applied in this region starting from year zero. Shaded parts indicate the periods during which sea surface temperatures and sea ice thickness are averaged and used as input for AGCM experiments.

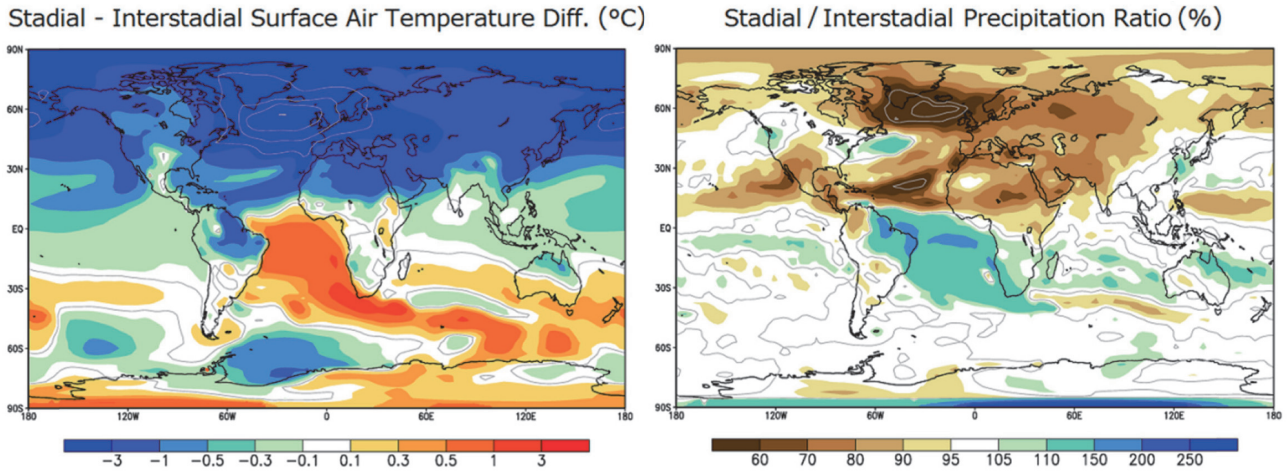

Fig. 2 Comparison of model stadial and interstadial climate: annual mean surface air temperature difference (left) and annual mean precipitation ratio (right). The model interstadial climate is taken to be that sometime after freshwater forcing is stopped.

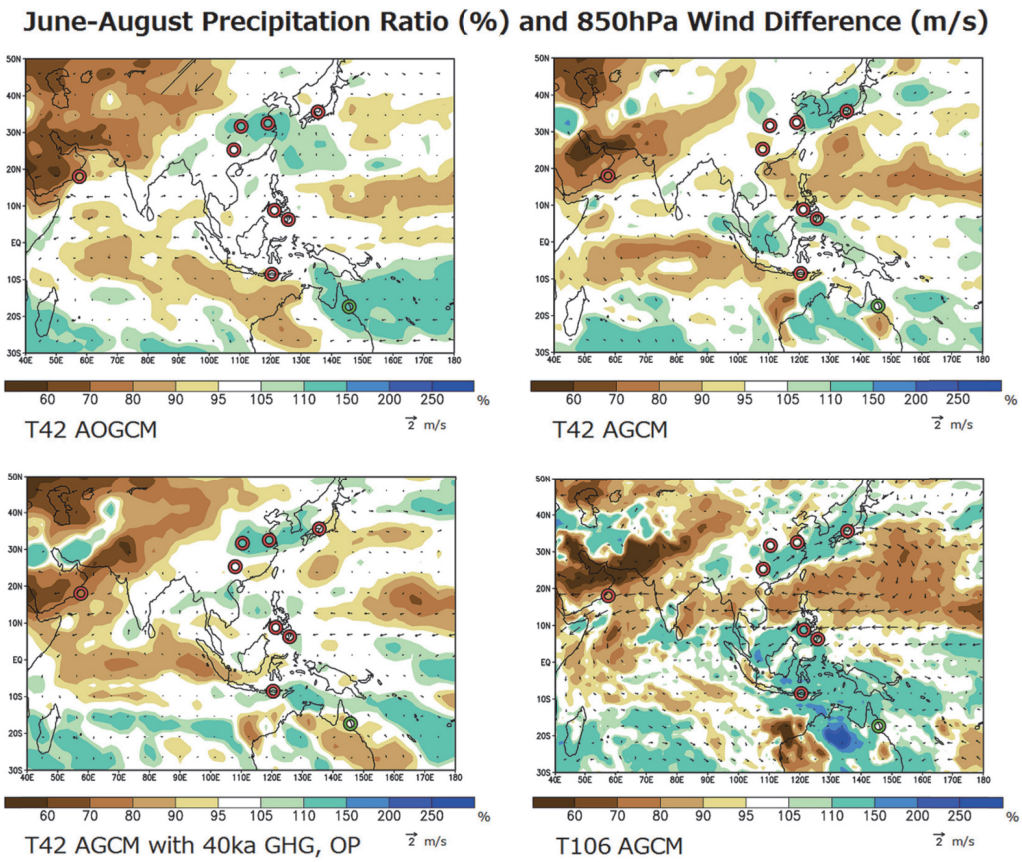

Fig. 3 Stadial/interstadial precipitation ratio and 850 hPa stadial-interstadial wind difference during June to August for different model configurations. The original AOGCM used 15ka orbital parameters and greenhouse gas configurations, but 40 ka configuration is applied to the medium resolution atmosphere model in the bottom right figure. Red circles indicate locations where proxy data indicate wetter conditions during typical stadial states.

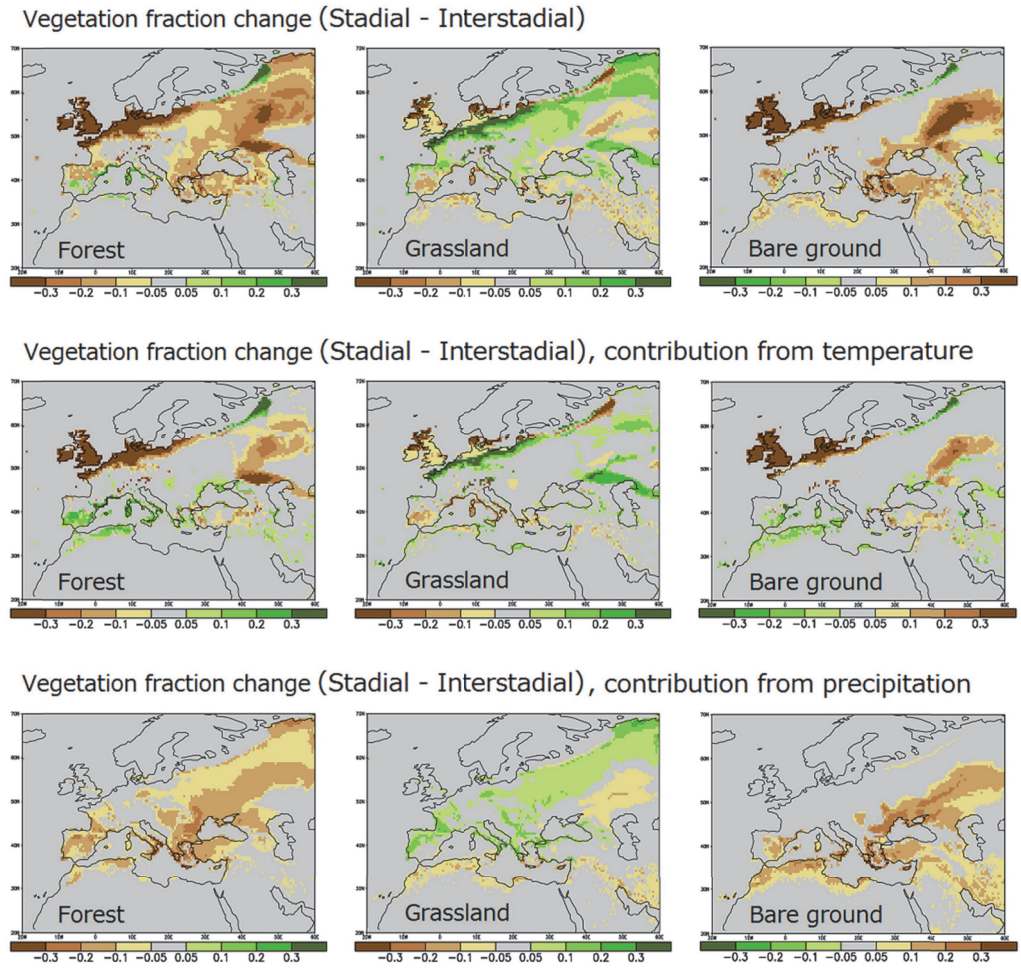

Fig. 4 Change in vegetation fraction from interstadial to stadial climates (top row), the change when only stadial temperature is applied to the DGVM (middle row), and the change when only stadial precipitation is applied (bottom row). Here, stadial temperature and precipitation are taken from the mid-resolution AGCM experiment.

forest PFTs. Precipitation is, however, of greater importance over northern Spain, western France and eastern Europe where it contributes to an increase in grassland. More specifically, lower precipitation leads to a decrease in temperate forests of southern Europe and in boreal forests of eastern Europe.

1.2 Vegetation change between stadial and interstadial

A vegetation coupled AGCM [3] is applied to introduce vegetation-climate feedback into paleovegetation prediction. In this vegetation coupled AGCM, vegetation distribution is also predicted to be consistent with temperature, precipitation and cloud cover in an experiment. The stadial- and interstadial-like sea surface temperature and sea ice distribution are used as boundary conditions. The predicted vegetation distributions in the interstadial (Fig. 5b) and stadial (Fig. 5c) show gradual changes from pre-industrial (warmer; Fig. 5a) to the LGM (colder; Fig. 5d). The largest difference between vegetation of the stadial and interstadial is shown in Europe. In other regions, vegetation distributions during stadial and interstadial is not so different. This result is consistent to previous study which classifies global vegetation from paleo evidences [4].

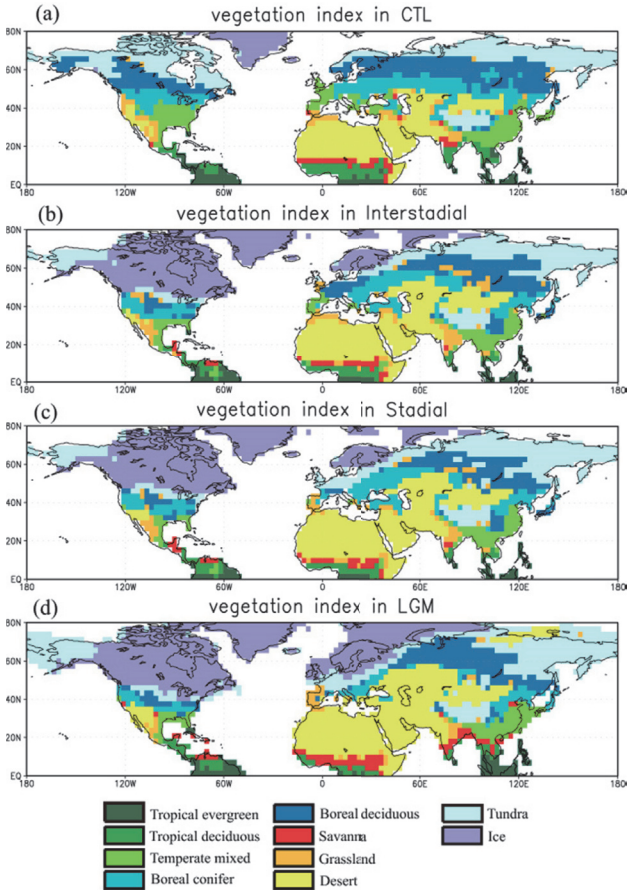

Fig. 5 Vegetation distribution in (a) the Pre-Industrial control, (b) Interstadial, (c) Stadial and (d) the Last Glacial Maximum obtained from vegetation coupled GCM experiments.

2. Influence of glacial ice sheets on Atlantic meridional overturning circulation through atmospheric circulation change under glacial climate

It is well known that glacial ice sheets (Laurentide, European, Antarctic ice sheets) have large influence on climate. Recently, several AOGCM studies suggested that glacial ice sheets exert a large impact on the AMOC [5]. However, the process by which the ice sheets impact on the AMOC is not yet fully understood because of the complicated nature of the AOGCMs. On the other hand, recent oceanographic studies showed that surface wind changes play a crucial role on changes to the AMOC under glacial climate [6]. Therefore, in this study, in order to interpret the results of the AOGCMs, we investigate in detail, the process by which the ice sheet modifies the AMOC through surface wind change. Here we conduct numerical experiments using an AGCM and an ocean general circulation model (OGCM) separately. Our method consists of 2 steps. First, from AGCM experiments, we evaluate the effect of glacial ice sheets on the surface wind. Second, from OGCM experiments, we evaluate the influence of the wind stress change on the AMOC by applying the surface wind change as a boundary condition, while leaving other boundary conditions (surface heat and water fluxes) unchanged. In this way, we can evaluate the wind effect of glacial ice sheet on the AMOC.

We find that glacial ice sheets largely intensify the AMOC by changing the surface wind field under glacial climate. From additional experiments, the wind change at North Atlantic mid-high latitudes appears to be particularly important. In this

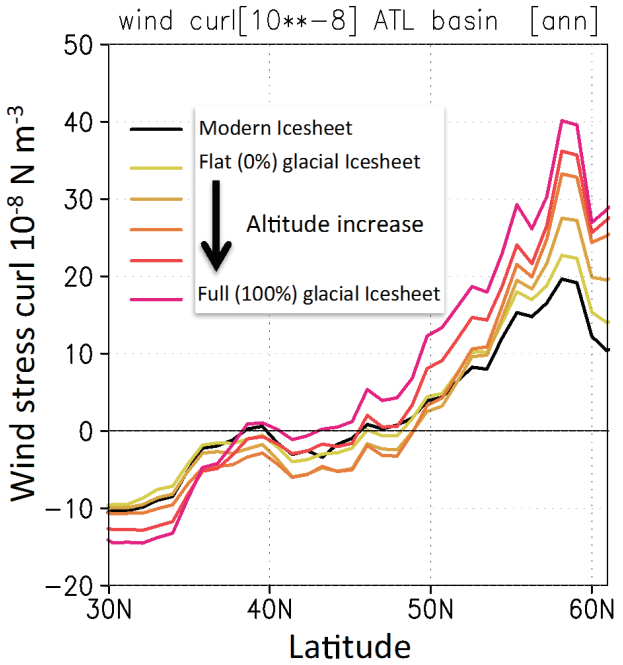

Fig. 6 Zonal mean wind stress curl over the Atlantic basin (unit: 10^{-8} N m^{-3}) for Modern Ice sheet configuration (black contour), with flat (0%) glacial ice sheet (yellow) and with full (100%) glacial ice sheet (pink). The percentage indicates the hight of the glacial ice sheets. The altitude of the ice sheet increases as the color of the contour gets redder.

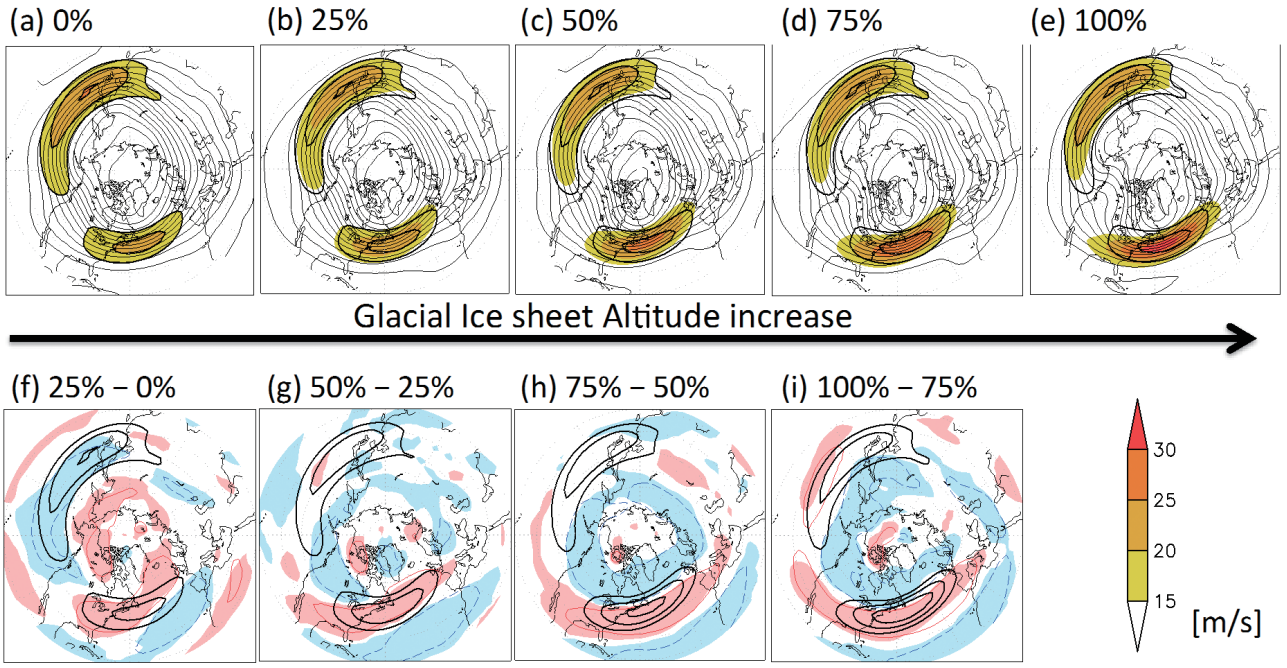

Fig. 7 Annual mean atmospheric circulation field at 500 hPa from glacial ice sheet linear altitude experiment. Top panel, (a)~(e), shows the annual mean climatological zonal wind (shade; m/s) and geopotential height (thin contour; m) for each experiment and zonal wind of (a) in bold contour. The number at the top indicates the percentage of the glacial ice sheet altitude. Bottom panel, (f)~(i), shows the difference of the zonal wind in red/blue contour, which indicates 1/-1 m/s change in the westerly; (f)=(b)-(a), (g)=(c)-(b), (h)=(d)-(c), (i)=(e)-(d). Shade indicates the 95% significance of the anomaly field based on Student t test and bold contour shows the climatology of zonal wind of 0% in (f), 25% in (g), 50% in (h) and 75% in (i).

region, the positive wind stress curl is enhanced as the glacial ice sheet altitude increases (Figs. 6 and 7). This contributes to an increase in surface salinity and surface temperature in the northern North Atlantic by strengthening the gyre circulation and the vertical mixing. Since the salinity change is the more dominant factors in seawater density when the ocean is cold, the surface density increases, and thus the stratification weakens in this region. Moreover, the increase in sea surface temperature induces sea ice retreat, which results in stronger heat exchange between the ocean and the atmosphere. As a result of these two effects, the AMOC intensifies. Our results suggest that the expansion of the glacial ice sheets over the last glacial period enhances the AMOC through modification of the surface wind field.

3. Changes in ocean circulation and dissolved oxygen under long-term global warming

Oceanic oxygen concentration is expected to decrease under anthropogenic climate change and past warmer climate conditions [7]. Reduction in oxygen solubility due to surface warming, enhanced stratification and reduced ventilation due to slower thermohaline circulation will tend to decrease the supply of oxygen to the ocean interior and to allow more biological oxygen utilization from an increase in the residence time of deep water, causing oxygen level to decline. Oxygen reduction is expected to persist for a thousand years or more, even after atmospheric carbon dioxide stops rising. However, there is less knowledge concerning long-term changes in oxygen concentration and circulation, because most future projections using sophisticated Earth system models with coupled AOGCM were only performed up to 2100.

Here, we simulate multi-millennial changes in ocean circulation and oxygen with doubling and quadrupling of atmospheric carbon dioxide, using MIROC3.2.3 and offline biogeochemical model. We increased the atmospheric CO_2 concentration by 1% per year from the pre-industrial value until it reached 2 × CO_2 and 4 × CO_2 levels at 70 and 140 years, respectively, and the value remained constant thereafter. Both experiments were integrated for 2000 years and reached a quasi-equilibrium state.

In the first 500 years, global mean O_2 concentration decreases from a pre-industrial value of 165.5 μmol/L to 149.5 (158.2) μmol/L in 4 (2) × CO_2 experiments (Fig. 8a). The projected oxygen reduction is comparable to CMIP5 models results [8]. However, after that, oxygen concentration in the deep ocean recovers globally and overshoots to preindustrial conditions, despite surface oxygen decrease and weaker Atlantic meridional overturning circulation (the present main driver of oxygen supply into the deep ocean) (Fig. 8b). The oxygen increase begins in the Southern Ocean between the subsurface and deep waters in association with recovery and overshoot of AABW (Fig. 8a,c). The strengthened AABW enhances ventilation and supplies oxygen-rich surface waters to the deep ocean. The oxygen-rich deep waters are transported into the other deep oceans and cancel out the oxygen reduction. At the end of the warming experiments, the strengthened AABW enhances

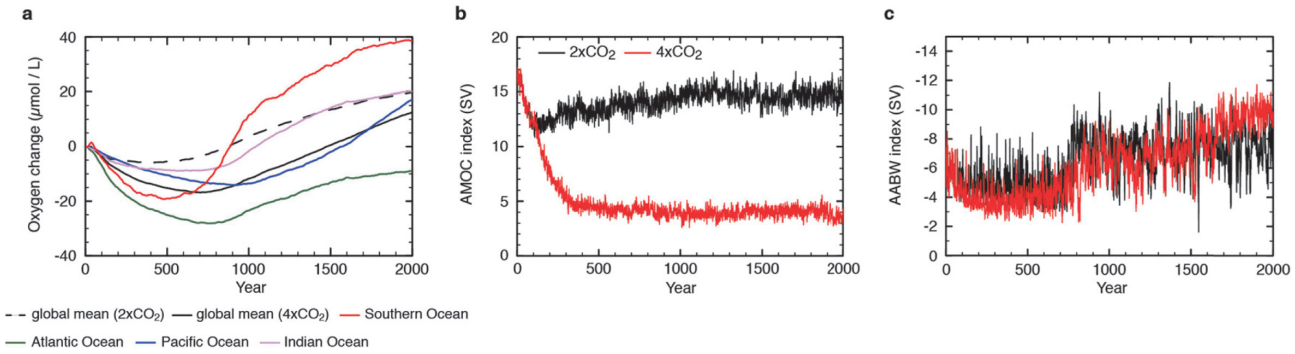

Fig. 8 Time series of change in dissolved oxygen concentration from pre-industrial conditions for the global mean (black solid), the Southern Ocean (red), the Atlantic Ocean (green), the Pacific Ocean (blue) and the Indian Ocean (purple) in the 4 × CO_2 experiment and global mean in the 2 × CO_2 experiment (black dashed). The projected global mean O_2 concentration in the pre-industrial condition is 165.5 μmol/L. Annual time series of AMOC index (**b**) and AABW index (**c**) for the 2 × CO_2 experiment (black) and the 4 × CO_2 experiment (red).

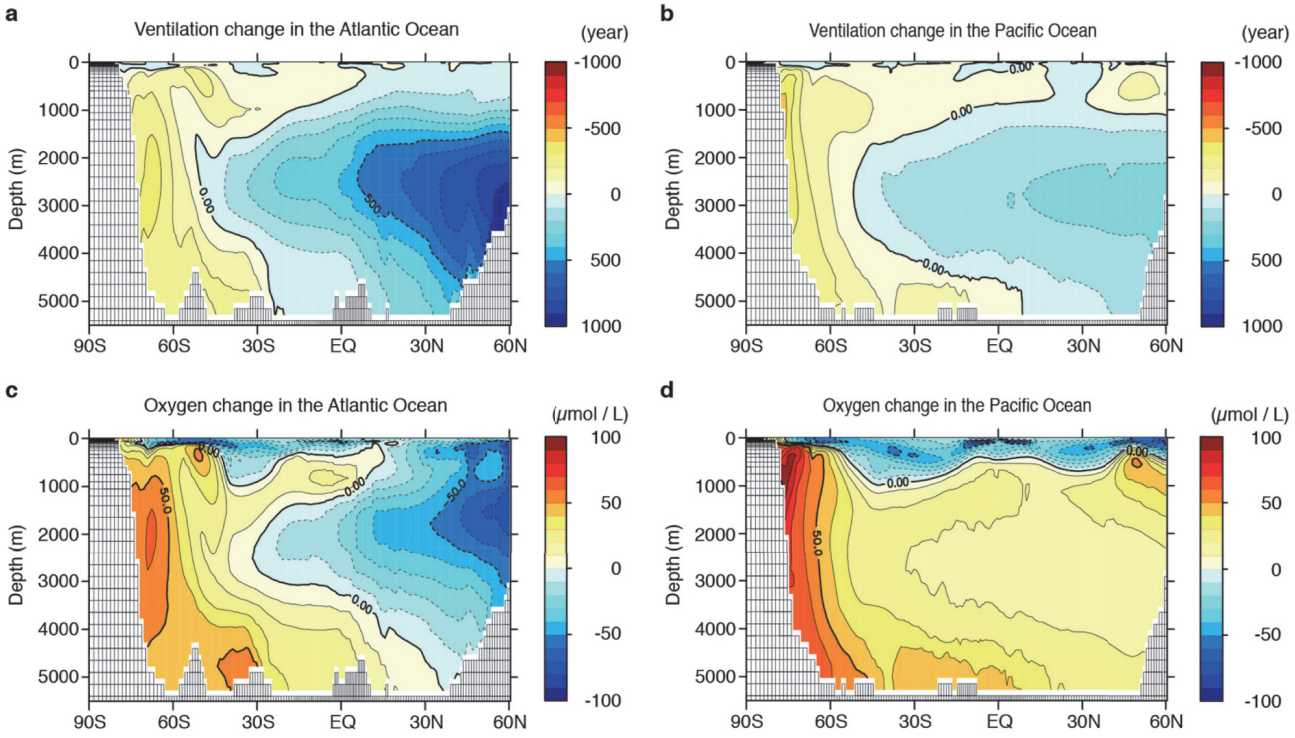

Fig. 9 Zonal mean change in ideal ocean age from pre-industrial conditions in the Atlantic Ocean (**a**) and Pacific Ocean (**b**). Cold colors represent older waters; warm colors represent younger waters. Zonal mean change in dissolved oxygen concentration from pre-industrial conditions in the Atlantic (**c**) and Pacific Oceans (**d**).

ventilation in most of the Southern Hemispheric deep ocean, mainly driving oxygen recovery and overshoot in the deep ocean (Fig. 9). Our results indicate that the change in ocean circulation in the Southern Ocean potentially drives millennial-scale oxygenation in the deep ocean, which is opposite to the centennial-scale global oxygen reduction.

4. Basal melting of the Antarctic ice sheet

Since the volume of the Antarctic Ice Sheet affects global sea level, investigating the nature and stability of the Antarctic ice sheet is required to constrain future sea level rise. Basal melting of the Antarctic ice shelves is an important factor in the retreat of marine Antarctic ice sheet in the past or future [9], but little consensus exists on how the rate of basal melting changes against climatic forcing. We simulate basal melting of Antarctic ice shelves under LGM and CO_2 doubling climate as well as present-day using a high-resolution ocean model [10] forced by outputs of a coupled climate model MIROC. In this set of experiments with a high-resolution ocean model, identical present-day ice shelf and ice sheet configuration is used to investigate the role of climatic forcing on the rate of basal melting. The model shows that above the continental shelf, the ocean temperature, which determines basal melting of ice shelves, does not change synchronously with that of the Southern Ocean. Active sea ice production in the Antarctic coast forms cold and dense shelf water, which prevents intrusion of warm deep water originating from the Southern Ocean onto continental shelves under a colder climate and present-day climate. Under a warmer climate, reduced sea ice production enables warm deep water to intrude onto continental shelves,

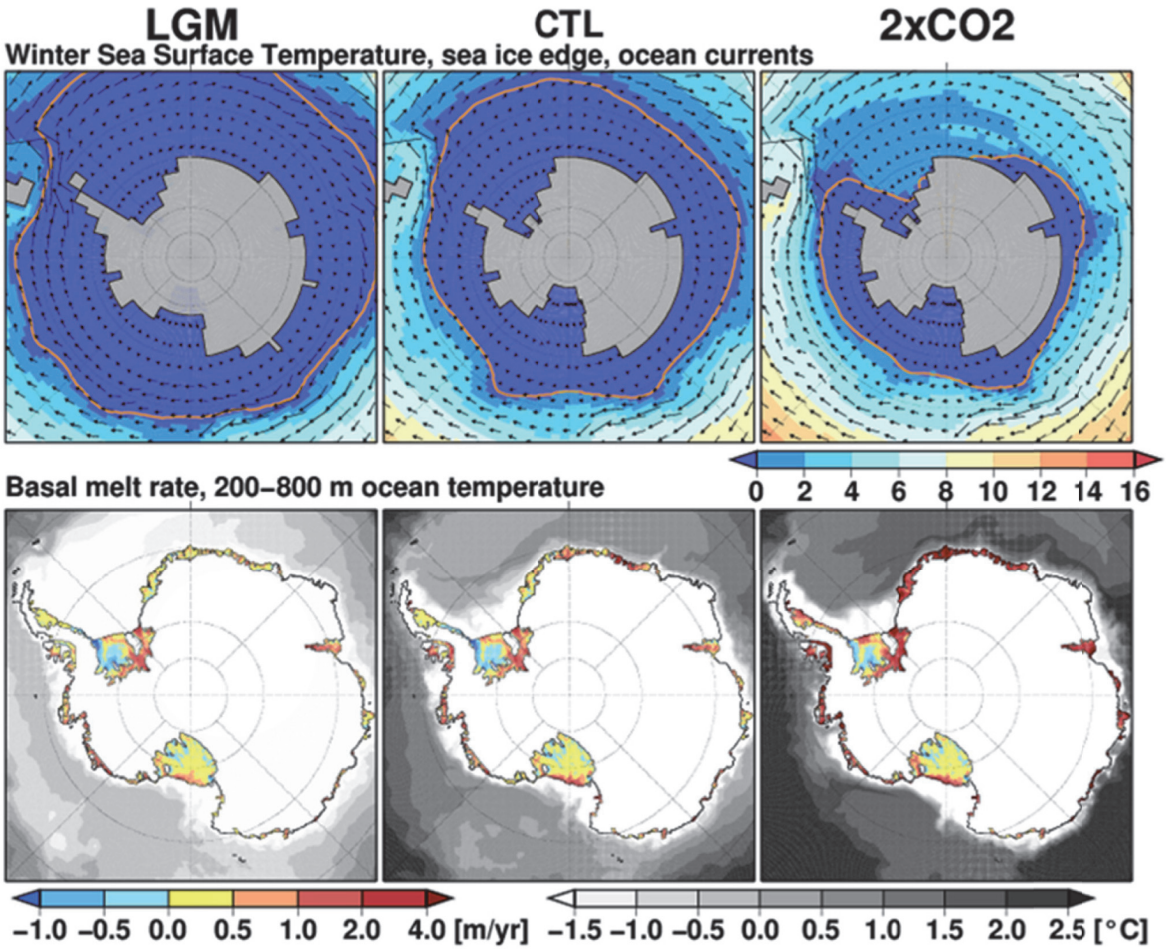

Fig. 10 (Top) Sea surface temperature, sea ice extent and ocean currents in the Antarctic region under the Last Glacial Maximum climate, present-day climate, and CO2 doubling climate simulated by MIROC. (Bottom) Spatial distributions of basal melt rate of ice shelves and subsurface ocean temperature simulated by the high-resolution ocean model.

which leads to increased basal melting. As a result, the change in the amount of basal melting amount in the CO_2 doubling climate is much larger than that in the LGM although the magnitude of global radiative forcings in the LGM and double CO_2 climate are similar (Fig. 10). Sensitivity experiments quantify the contributions from individual climatic components and show that contributions from sea surface heat flux and deep ocean temperature are important for basal melting.

References

[1] North Greenland Ice Core Project members, High-resolution record of Northern Hemisphere climate extending into the last interglacial period. *Nature*, **431**, 147–151, 2004.

[2] Müller, U. C., Pross, J., Tzedakis, P. C., Gamble, C., Kotthoff, U., Schmiedl, G., Wulf, W., and Christianis, K., The role of climate in the spread of modern humans into Europe. *Quat. Sci. Rev*, **30**, 273–279, 2011.

[3] O'ishi, R. and Abe-Ouchi, A., Polar amplification in the mid-Holocene derived from dynamical vegetation change with a GCM. *Geoph. Res. Lett*., **38**, L14702, 2011.

[4] Harrison, S. P. and Sanchez-Goñi, M. F., Global patterns of vegetation response to millennial-scale variability and rapid climate change during the last glacial period. *Quat. Sci. Rev*., **29**, 2957–2980, 2010.

[5] Smith, R. S. and Gregory, J., The last glacial cycle: transient simulations with an AOGCM. Climate Dynamics, **38**,1545–1559, 2912.

[6] Oka, A., Hasumi, H., and Abe-Ouchi, A., The thermal threshold of the Atlantic meridional overturning circulation and its control by wind stress forcing during glacial climate. *Geoph. Res. Lett*., **39**, 6, 2012.

[7] Keeling, R. F., Körtzinger, A., and Gruber, N., Ocean deoxygenation in a warming world. *Ann. Rev. Mar. Sci*., **2**, 199–229, 2010.

[8] Bopp, L. *et al*., Multiple stressors of ocean ecosystems in the 21st century: projections with CMIP5 models. *Biogeosciences*, **10**, 6225–6245, 2013.

[9] Pollard, D. and DeConto R. M., Modelling West Antarctic ice sheet growth and collapse through the past five million years. *Nature*, **458**, 329–332, 2009 .

[10] Kusahara, K. and Hasumi, H., Modeling Antarctic ice shelf responses to future climate changes and impacts on the ocean. *J. Geophys. Res.-Oceans*., **118**, 2454–2475, 2013.

古環境研究のための多階層数値実験

課題責任者
阿部　彩子　　東京大学　大気海洋研究所

著者
阿部　彩子 *1，吉森　正和 *2，Wing-Le Chan*1，山本　彬友 *1，尾崎　和海 *1，大石　龍太 *3，
新田　友子 *1，小長谷貴志 *1，シェリフ多田野サム *1，Alexandre Laine*3，大垣内るみ *4，高橋　邦生 *5，
濱野　勇臣 *2

∗1 東京大学　大気海洋研究所
∗2 北海道大学　大学院地球環境科学研究院
∗3 情報・システム研究機構　国立極地研究所
∗4 海洋開発研究機構　気候変動リスク情報創生プロジェクトチーム
∗5 海洋開発研究機構　統合的気候変動予測研究分野

大気海洋結合モデル MIROC4m を用いて、北大西洋への淡水流入実験を行い、地質学的証拠が示す数千年スケールの亜氷期－亜間氷期の気候変動と整合的な結果を得た。また、高解像度モデル MIROC3h で亜氷期の急激な気候変動を再現するためのダウンスケーリング手法を開発した。植生結合した MIROC-LPJ を用いて亜氷期と亜間氷期の気候と植生の再現実験を行った結果、地質学的証拠が示す古植生変動と整合的な結果を得た。

大気海洋大循環モデルを用いて行われた現在実験と氷期実験の結果と単独の大気モデル・海洋モデルを併用し、氷期氷床の存在が大西洋子午面循環に与える影響を調べた。その結果、氷床が風成循環を通して大西洋子午面循環を強化することが明らかになった。

温暖化による海水中の酸素濃度への長期的な影響を見積もるため、MIROC4m を用いて行われた大気二酸化炭素 2 倍増および 4 倍増実験結果を用いた推定を行った。その結果、初期の 500 年は全球的に海洋酸素濃度が減少し、その後で産業革命前よりも高酸素濃度に回復した。これは南大洋での深層水形成活発化に伴うもので、温暖化に対する海洋循環と酸素の変動が数百年スケールと千年スケールで異なる可能性が示された。

気候変化が南極氷床の底面融解に与える影響を調べるため、大気海洋結合モデルの結果を境界条件として南大洋を領域とした高解像度海洋大循環モデルを用いた数値実験を行った。その結果、最終氷期極大期と大気二酸化炭素倍増では産業革命前と比較して放射強制力の差は同程度にもかかわらず、大気二酸化炭素倍増時と産業革命前の底面融解の差は最終氷期と産業革命前のそれと比べてはるかに大きいという非線形な応答が示された。

キーワード: 大気海洋大循環モデル MIROC, 古気候モデリング, 最終氷期, 亜氷期－亜間氷期, 海洋溶存酸素, 氷床底面融解